

## **EUM-WP-22 SURFACE ALBEDO FROM GEOSTATIONARY SATELLITES**

This paper investigates the possibility to derive a spatially consistent broadband surface albedo product from different geostationary spacecrafts. In this context, 10 days of data from GOES-8, -10 and GMS-5 dated of May 2001 have been delivered to EUMETSAT. The consistency analysis relies on the comparison of albedo derived over the common areas observed by adjacent satellites. So far, one ten-day period of data acquired by these satellites has been processed as a demonstration phase. Together with data from Meteosat-5 and -7 this provides the first “global view” of a geostationary surface albedo product. This paper closes the work offered by EUMETSAT in response to Action 31.27 and 31.28. The surface albedo retrieval algorithm could be made available to the CGMS members upon request for the processing of their own archived data.

## EUM-WP-22 Surface Albedo from Geostationary Satellites

### 1 INTRODUCTION

Observations from operational meteorological satellites, composed both of polar-orbiting and geostationary platforms, play an increasing role in documenting climate variations thanks to the duration of their respective archive, often covering more than two decades (Ohring and Gruber 2001). During the late seventies and early eighties, space-borne observations of the Earth were very scarce, essentially limited to geostationary meteorological observations and a few polar platforms. The instruments onboard these satellites as well as their routine operation procedures were however not originally conceived to support the objectives of climate monitoring. Consequently, a number of basic issues like uncontrolled orbit drift, geo-rectification accuracy or poorly calibrated and characterized sensors need to be addressed prior to any climate exploitation of these data. Nevertheless, observations acquired by these instruments have already proven to be useful in a number of areas such as atmospheric temperature (e.g., Christy et al. 2000), sea surface temperature (e.g., Strong et al. 2000), or cloud cover (Rossow et al. 1985), though those applications are still subject to controversial debates. As concerns land surface characterization, snow cover (e.g., Robinson 2000), vegetation indices and the Fraction of Absorbed Photosynthetically Active Radiation (FAPAR) or surface albedo (e.g., Ba et al. 2001) are typical parameters that have been derived from meteorological satellites.

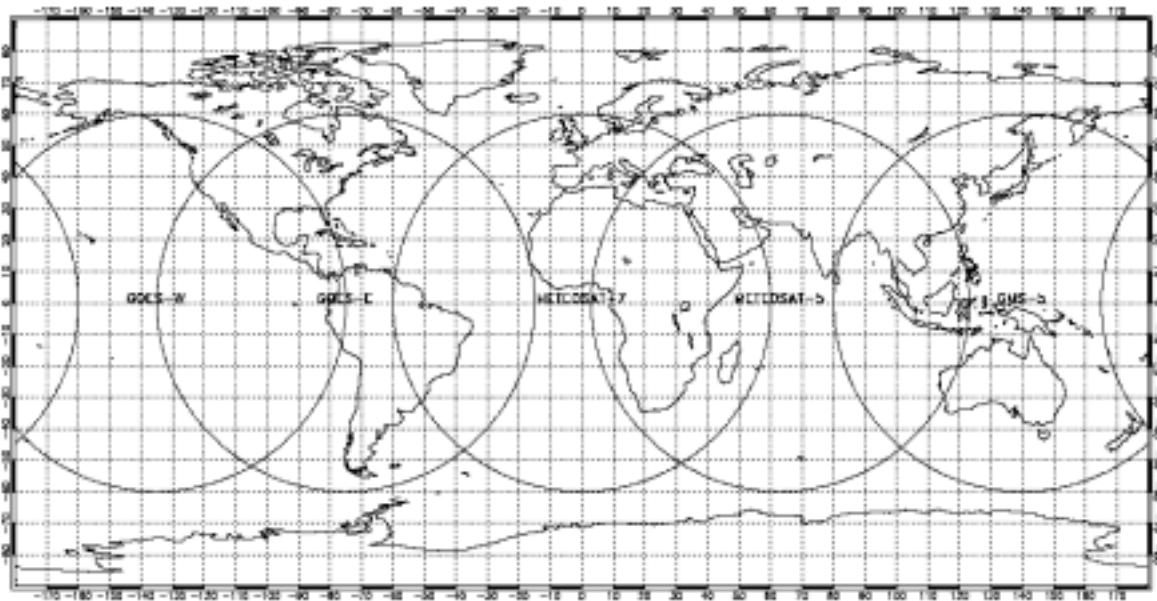


Figure 1: Location of operational geostationary satellites used in this study. Circles show the 60° viewing angle limit.

Among these parameters, the albedo of the Earth's surface is a critical variable for climate studies, as it controls the fraction of solar energy available to the surface (e.g., Dickinson 1983). Although the potential of space-based observations to derive globally surface albedo maps has long been recognized, it is routinely retrieved only since 2001 from radiometers onboard the Terra platform (Jin et al. 2003; Martonchik et al. 1998).

Consequently, inter-annual surface albedo variability and its impact on the atmosphere, as predicted by Charney (1975), are still poorly quantified. This situation results in part from the scarceness of space instruments dedicated to land surface observations before the late 1990s, when systematic space-borne observations of the land surface were essentially limited to data acquired by geostationary meteorological satellites and a few polar platforms. Nevertheless, Pinty et al. (2000b) demonstrated the potential of geostationary satellites for the generation of reliable surface albedo maps. The high temporal sampling of geostationary satellites allows to account for both the atmospheric scattering effects and the anisotropy of the surface reflectance when data are accumulated during the course of the day (Pinty et al. 2000a). This novel approach opens thus new avenues for the exploitation of geostationary satellite observations for climate studies since their corresponding archives often cover two decades or more. A single geostationary satellite only observes a part of the globe, limited to an area of about  $\pm 60^\circ$  around the sub-satellite point. A global view of the Earth from the geostationary orbit, with the exception of the poles, is ensured by a suite of operational meteorological satellites located at regular intervals along the Equator. The missions and performances of these spacecrafts are technically and operationally coordinated by the committee for the Coordination of Geostationary Meteorological Satellites (CGMS). This paper investigates the possibility to derive spatially consistent surface albedo product from different geostationary satellites. Data acquired in May 2001 by five different geostationary satellites, namely Meteosat-7, -5, Geostationary Meteorological Satellite (GMS-5) and Geostationary Operational Environmental Satellite (GOES-8/10) have been used for this demonstration study. The consistency analysis of this product relies on the comparison of albedo derived over the common area observed by two adjacent satellites (Govaerts et al. 2004). Results from this consistency analysis are presented in this paper.

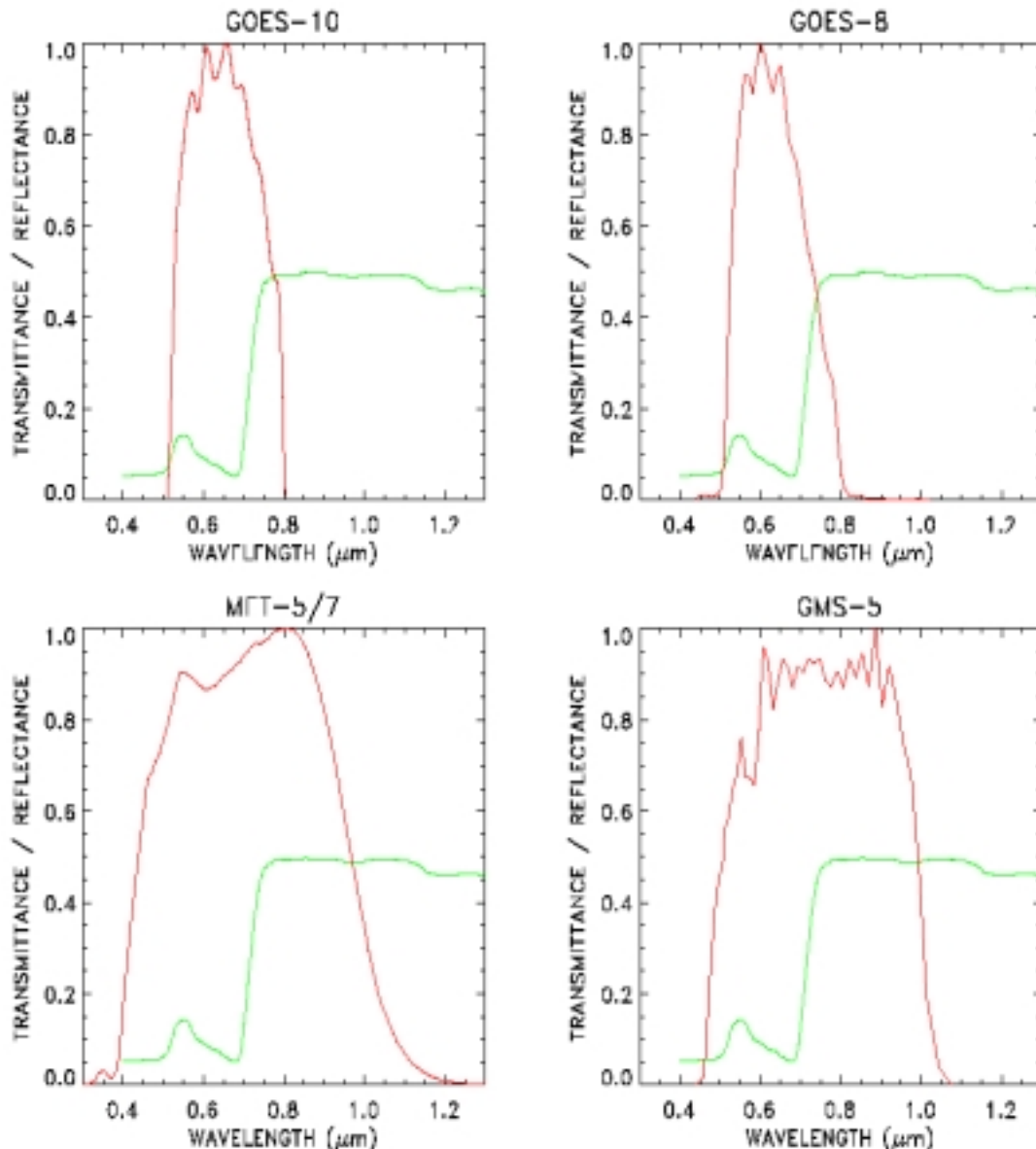


Figure 2: Sensor Spectral Response (SSR) of the geostationary VIS band radiometer used in this study (red line). The green solid line illustrates typical reflectance of green vegetation.

## 2 RADIOMETER CHARACTERISTICS

The location of the geostationary weather satellites used in this study is shown on Figure (1). All radiometers onboard these instruments observe the Earth with a broad solar channel, referred to as the VIS band, ranging approximately from 0.6 up to 0.8  $\mu\text{m}$  (Figure 2). Vegetated surface reflectance exhibits quite strong and fast spectral variations over this spectral region as a consequence of the differences in the radiation transfer regimes occurring on both sides of 0.7  $\mu\text{m}$  that is, mainly governed by absorption (scattering) at wavelengths shorter (larger) than 0.7  $\mu\text{m}$ . As can be seen on Figure (2), the VIS band of the Meteosat Visible and InfraRed Imager (MVISR) and Visible Infrared Spin-Scan Radiometer (VISSR) onboard GMS have similar shape and encompasses both side the vegetation spectral regimes. Conversely, the VIS band onboard the GOES Imager essentially cover the absorption part of

the vegetation and has only limited sensitivity to the scattering regime region. The main characteristics of the radiometers used in this study are summarized in Table (1).

Location	Satellite	Sensor	Irr <sup>(a)</sup> Wm <sup>-2</sup>	Rep. C. <sup>(b)</sup> min	Scan. <sup>(c)</sup> Scan.	S. Dist. <sup>(d)</sup> km	N. D. <sup>(e)</sup>	Digit. <sup>(f)</sup> Bits
135 <sup>oW</sup>	GOES-10	Imager	313	~30 <sup>(g)</sup>	N-S	1	9	10
75 <sup>oW</sup>	GOES-8	Imager	364	~30 <sup>(g)</sup>	N-S	1	9	10
0 <sup>o</sup>	Meteosat-7	MVIRI	691	30	S-N	2.5	2	8
63 <sup>oE</sup>	Meteosat-5	MVIRI	691	30	S-N	2.5	2	8
140 <sup>oE</sup>	GMS-5	VISSR	708	60	N-S	1.25	4	6

Table 1: Characteristics of the radiometer onboard the geostationary spacecraft shown on Fig. (1) operational in May 2001. (a) Exo-atmospheric irradiance in the spectral response. (b) Repeat cycle available from the archive. (c) Scanning mode. (d) Sampling distance at the sub-satellite point. (e) Number of detectors. (f) Digitalization levels. (g) The images do not cover the full disk at that frequency.

### 3 CONSISTENCY ANALYSIS METHOD

#### 3.1 Calibration consistency verification

Top-of-Atmosphere (TOA) Bidirectional Reflectance Factors (BRFs) constitutes the basic input of the surface albedo retrieval algorithm (Pinty et al. 2000a). It is therefore necessary to verify the calibration consistency between adjacent satellites prior to perform surface albedo consistency analysis. To this end, satellite images have been first calibrated in radiance, using the coefficients given by Govaerts et al. (2004) for Meteosat, Minnis et al. (2002) for GMS-5, Nguyen et al. (2004) for GOES-10 and finally Le Borgne et al. (2004) for GOES-8.

These TOA radiances have next been converted in BRFs using the irradiance values given in Table (1). For each adjacent instruments, TOA BRFs acquired over homogeneous areas of about 20 x 20 km in size with identical viewing zenith angles and differences in sun zenith angles not exceeding  $\pm 2^\circ$  have been compared. These homogeneous collocated areas are disposed along a longitudinal transect centered between the two sub-satellites points. Data from the East side of a pair of adjacent satellites have been converted to account for the spectral difference with the West side radiometer. For each collocated areas, the relative difference  $d_r$  is computed with respect to the West satellite with

$$d_r = 100 \frac{I^E - I^W}{I^W} \quad (1)$$

where  $I^E$  and  $I^W$  are the pair of collocated TOA BRFs of the East and West satellites respectively.

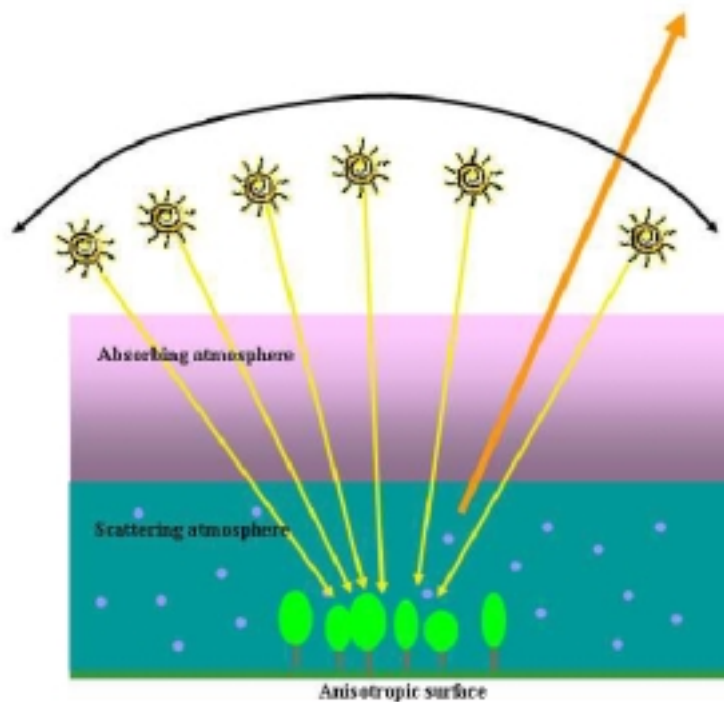


Figure 3: Schematic representation of the Geostationary Surface Albedo (GSA) algorithm concept. The forward model is composed of an upper absorbing gaseous layer and a lower scattering one inverted against daily accumulation of observations acquired at different illumination angles.

### 3.2 Surface albedo verification

Surface albedo, or more precisely Directional Hemispherical Reflectance (DHR), have been derived for each radiometer with the method proposed by Pinty et al. (2000a). This method accounts for the simultaneous characterization of surface anisotropy and atmospheric scattering properties, explicitly accounting for the radiative coupling between these two systems. The approach relies on a daily accumulation of geostationary observations in the VIS band under different illumination conditions to assess the scattering properties of the surface and the atmosphere (Figure 3). This algorithm assumes that i) surface and atmospheric scattering properties are constant throughout the day, ii) continental aerosol type are applicable everywhere and all year long, iii) surface anisotropy can be represented with the simple BRDF model proposed by Rahman et al. (1993) and finally iv) the Helmholtz reciprocity principle is valid over terrestrial surfaces at a spatial resolution of a few kilometers (Lattanzio et al. 2005). On a daily basis, the Geostationary Surface Albedo (GSA) algorithm estimates the DHR value for each pixel, corrected for atmospheric effects, for a Sun zenith angle fixed at  $30^\circ$ . A simple composite procedure is applied over consecutive 10-day periods to produce geographically complete maps of surface albedo (Pinty et al. 2000b). This retrieval is performed in the geostationary satellite projection. The GSA algorithm explicitly calculates the measurement error for each images and propagate this error in the retrieval scheme to provide an error estimate of the derived surface albedo.

Since observation areas observed by two adjacent satellites overlap as can be seen on Fig. (1), albedo comparison in this common region offers a unique opportunity to evaluate the consistency of a same product retrieved from two radiometers located at two different places (Govaerts et al. 2004). Each 10-day products have next been projected into a regular latitude/longitude grid, keeping only pixels with a reliable retrieval. All products have next been converted into a unique spectral interval ranging from 0.3 to 3.0  $\mu\text{m}$  (Govaerts et al. 2005) in order to generate a global broadband shortwave albedo map (Figure 4). Details concerning the retrieval process are given in Table (2). Gridded broadband surface albedos have been compared for each common area,

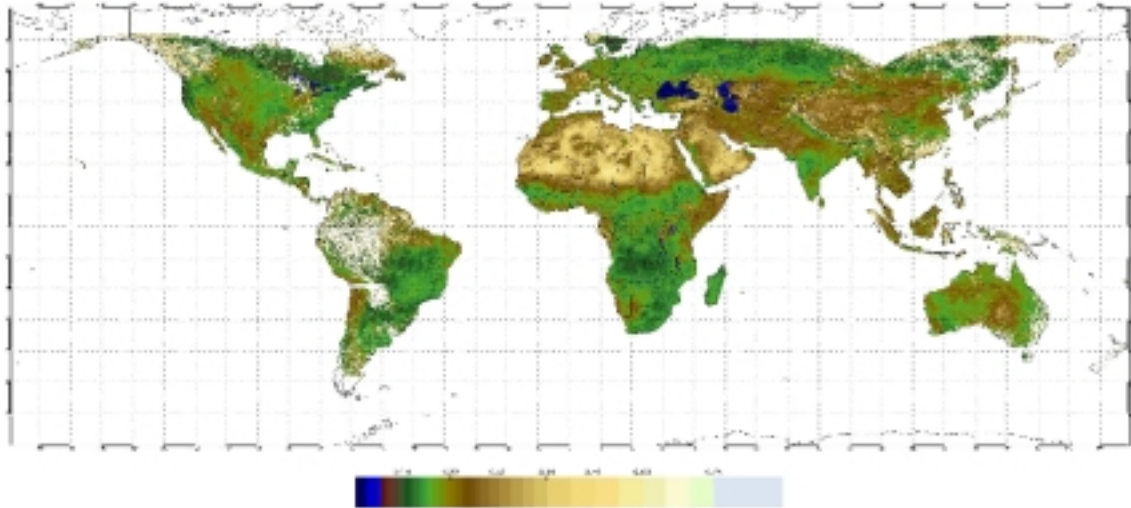


Figure 4: Gridded broadband surface albedo map derived at EUMETSAT with the GSA algorithm from Meteosat-5/-7, GMS-5 and GOES-8/10 observations acquired on May, 1-10, 2001.

Satellite	Nbr days	<Img/day>	<Meas. R. Err.>	<DHR R. Err>
<b>GOES-10</b>	<b>10</b>	<b>22.9<sup>(a)</sup></b>	<b>5.2%</b>	<b>12.5%</b>
<b>GOES-8</b>	<b>10</b>	<b>13.7<sup>(a)</sup></b>	<b>6.8%</b>	<b>14.4%</b>
<b>MET-7</b>	<b>10</b>	<b>17.3</b>	<b>7.4%</b>	<b>8.7%</b>
<b>MET-5</b>	<b>10</b>	<b>16.3</b>	<b>10.0%</b>	<b>10.1%</b>
<b>GMS-5</b>	<b>10</b>	<b>9.9</b>	<b>8.4%</b>	<b>10.5%</b>

Table 2: Number of days processed during the 1 - 10 May 2001 period for each satellite. <Img/day> is the mean number of images available per day. <Meas. R. Err.> is the mean measurement relative error, *i.e.*, including both the radiometric error and forward model uncertainty. <DHR R. Err.> is the mean estimated DHR relative error. (a) Not all images cover the full disk.

With the exception of GOES-10 and GMS-5 the common area of which almost does not encompass any land surfaces. The relative difference  $d_{\text{DHR}}$  between the East and the West DHR values, noted  $\text{DHR}_E$  and  $\text{DHR}_W$  respectively, is estimated for each grid point of the common area with

$$d_{\text{DHR}} = 200 \frac{\text{DHR}_E - \text{DHR}_W}{\text{DHR}_E + \text{DHR}_W} \quad (2)$$

## 4 RESULTS

### 4.1 GOES-10 vs. GOES-8

GOES-10 data were calibrated against radiances acquired by the self-calibrating sensor Visible Infrared Scanner (VIRS) onboard the Tropical Rainfall Measuring Mission (TRMM) platform (Nguyen et al. 2004). GOES-8 data were calibrated using Meteosat-7 VIS band radiances as reference (Le Borgne et al. 2004). Figure (5 A) shows the scatter-plot of GOES-10 and the relative difference between GOES-8 and -10 estimated with Equation (1). Over land surfaces, *i.e.*, where the TOA BRF is typically below 0.25, TOA BRFs of both radiometers agree within 1% relative difference despite they have been calibrated using different references.

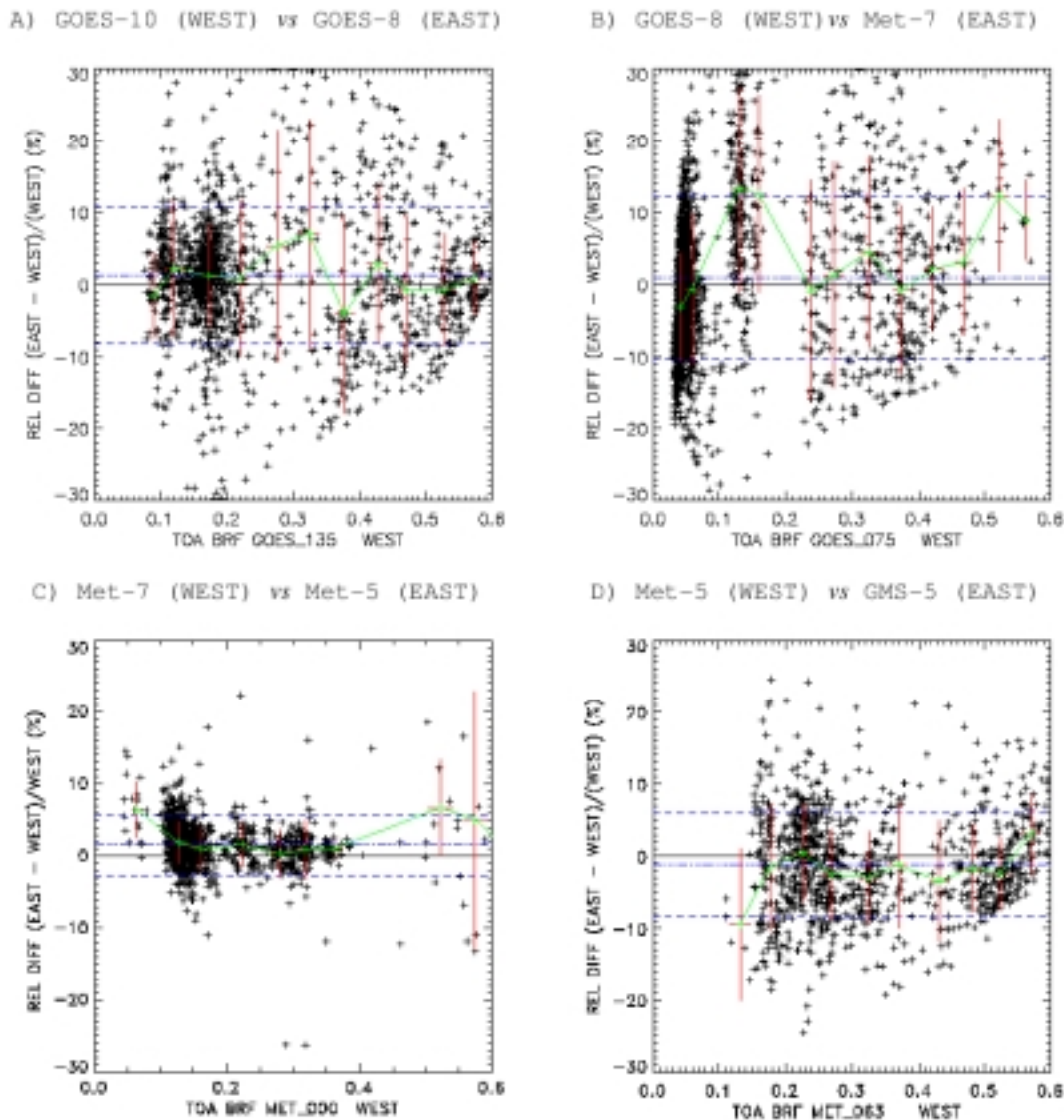


Figure 5: Comparison between the TOA BRFs for each pair of adjacent satellites along the longitudinal transect with identical viewing zenith angles and differences in sun zenith angles not exceeding  $\pm 2^\circ$ . The collocated TOA BRF relative difference between the East and West satellites (+ symbol) is expressed with respect to the West one. The mean relative difference is shown with the dash-dotted vertical line and its standard deviation with the dashed vertical line.

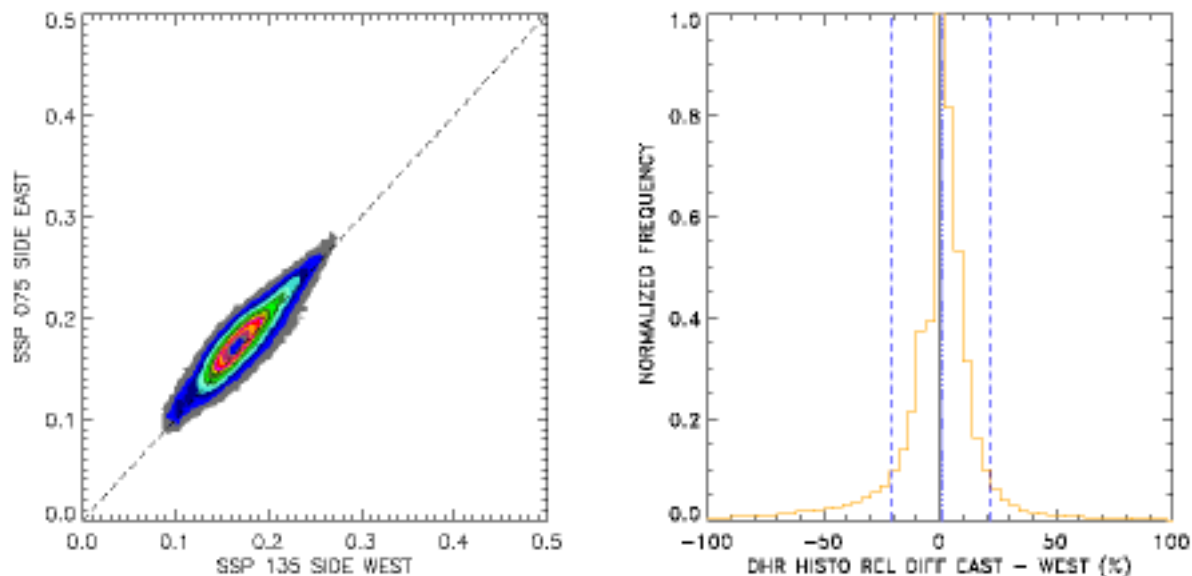


Figure 6: Comparison between GOES-10 (labelled SSP 135 SIDE WEST) and -8 (labelled SSP 075 SIDE EAST) broadband DHR over the common area. **Left:** broadband DHR density plot. **Right:** Histogram of the broadband DHR relative difference estimated with Equation (2). The blue vertical dash-dotted line represents the mean of the DHR relative differences and the blue vertical dashed lines its standard deviation.

		TOA	BRF	BB DHR	
Common	Area	Mean	Std	Mean	Std
GOES-10	- GOES-8	+1.3	9.5	+ 0.5	21.0
GOES-8	- Met-7	+1.0	11.0	+ 5.0	32.7
Met-7	- Met-5	+1.5	4.0	+ 1.9	18.6
Met-5	- GMS-5	-1.2	7.1	-11.1	32.7

Table 3: Results of the TOA BRF and broadband surface DHR comparisons.

Most of the Northern American continent up 50° N, Central America and the North-West part of South America are observed commonly by these two satellites. Broadband DHR comparison results are shown on Figure (6) and Table (4). There is a very good agreement between both products, with a mean relative difference that does not exceed the calibration difference.

#### 4.2 GOES-8 vs. Meteosat-7

Meteosat-7 data were calibrated with the coefficients distributed by EUMETSAT (Govaerts et al. 2004) derived from TAO radiance simulation over bright desert targets (Govaerts and Clerici 2004). Figure (5 B) shows the scatter-plot between GOES-8 and the relative difference estimated with Equation (1).

The common area seen by these two satellites is limited to the Eastern part of South America, a region essentially covered by dense vegetation. On the average, broadband surface albedo derived from Meteosat-7 overestimates by about 5% those derived from GOES-8 (Figure 7).

As stated in Section (2), the spectral response of both radiometers encompasses different part of the vegetation spectral regime with the GOES Imager sensing mainly the absorption regime. Consequently, the conversion of GOES results in broadband albedo includes some uncertainties, which translate into a larger standard deviation between the two surface albedo distributions (Table 4).

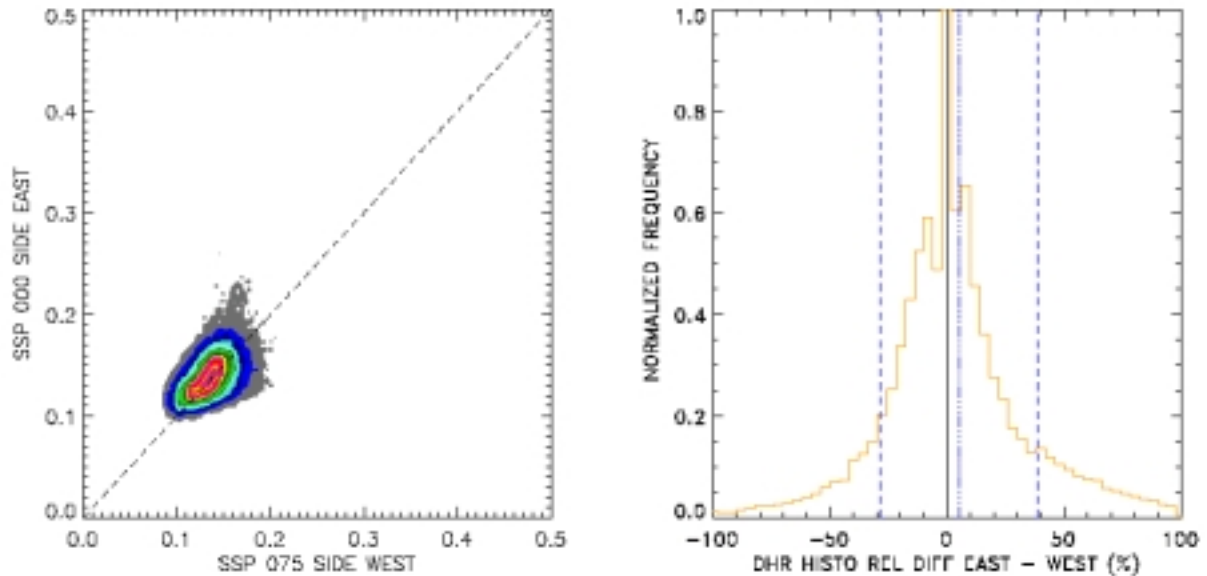


Figure 7: As Figure (6) but for GOES-8 (labelled SSP 075 SIDE WEST) and Meteosat-7 (labelled SSP 000 SIDE EAST).

### 4.3 Meteosat-7 vs. Meteosat-5

The characteristics of the Meteosat-5 and -7 radiometer VIS band should be, in principle, similar, as their detectors have been produced in the same batch and according to identical specifications. Both instruments are routinely calibrated with the same vicarious method that relies on simulated radiance over bright desert targets (Govaerts et al. 2004). There is a good agreement between the respective TOA BRFs as can be seen in Fig. (5 C). A detailed analysis of the relative difference between both signals over cloud free areas reveals however some discrepancy, in particular over dark sea surfaces, where the TOA BRF is close to 0.05 in the Meteosat VIS band. Such result might indicate some minor linearity problems with one of the two instruments as a 5% difference corresponds to about half a digital count value over sea surfaces. The sharp transition between sea and terrestrial surfaces, where the TOA BRF typically ranges from 0.1 to 0.4, rather advocates a possible Meteosat-5 spectral response error around 0.4 $\mu$ m, where spectral radiance over sea takes its maximum value.

Over terrestrial surfaces, observations are very consistent, Meteosat-5 reflectances overestimating only by about 10% those observed by Meteosat-7.

The area observed jointly by these two instruments encompasses most of the African continent, South-East of Europe and the Arabian peninsula, covering thereby a wide variety of surface types, ranging from dark swampy areas up to very bright deserts. There is a very good agreement between the surface albedo derived by these two satellites (Figure 7). The mean bias is in the range of the calibration difference and can thus be easily explained by the uncertainty in the characterization of the respective sensor spectral response.

#### 4.4 Meteosat-5 vs. GMS-5

GMS-5 data were calibrated against TRMM/VIRS radiances (Minnis et al. 2002). The GMS/VISSR VIS band has a non-linear response with respect to radiance which can be approximated by an exponential function. Meteosat-5 TOA BRFs slightly overestimated by about 1% those derived from GMS-5 (Figure 5 D). Bias in the DHR comparison is exhibiting the same trend, but is much larger as it exceeds 10%. The density plot on Figure (9) reveals a series of grid points which exhibits larger DHR values for Meteosat-5 than for the GMS-5, whereas most of the grid points have similar DHR values as can be seen from the histogram of the relative.

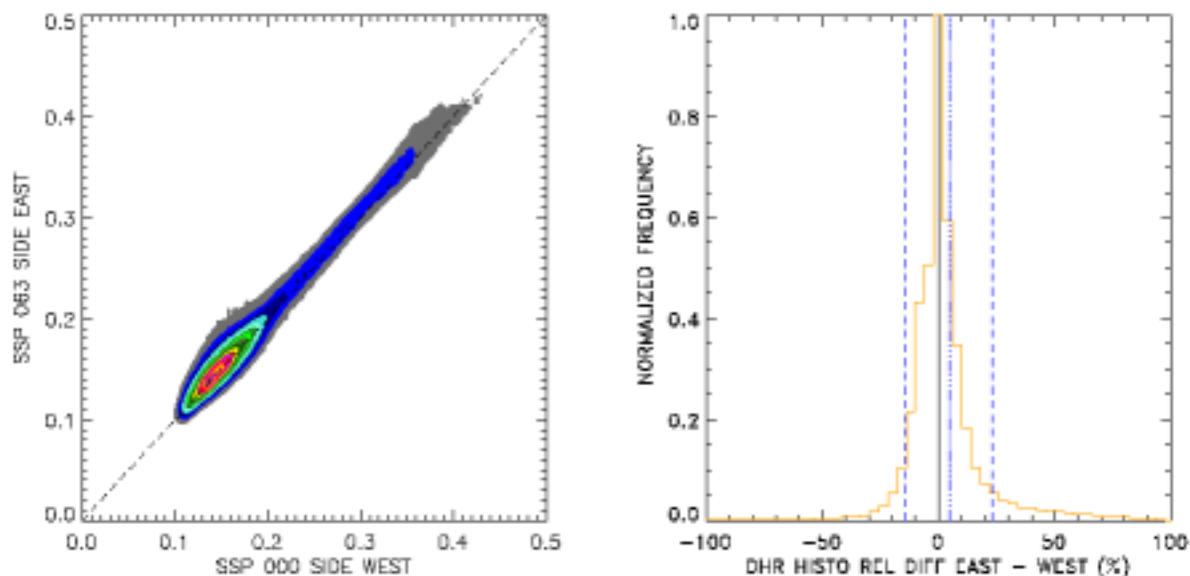


Figure 8: As Figure (6) but for Meteosat-7 (labelled SSP 000 SIDE WEST) and -5 (labelled SSP 063 SIDE EAST).

Difference (Figure 9). These points with albedo values higher for Met-5 than GMS-5 are due to residual cloud contamination on Meteosat-5 product.

## 5 CONCLUSIONS

Recently, the Global Climate Observing System (GCOS) committee recognized the need for establishing a benchmark for assessing land-surface albedo product and implementing a system for the retrieval of surface albedo from existing and archived geostationary satellites to form a global climatology of albedo for the entire period of available measurements (GCOS 2003). The results presented in this paper, triggered by CGMS action 31.27, constitute a first step in that direction. The VIS bands onboard Meteosat-7, -5, GMS-5, GOES-10 and -8 radiometers were not originally conceived to support quantitative applications, *i.e.*, without any strong requirements concerning the accuracy and precision of its calibration. Their calibration appears however fairly consistent, despite their reliance on different calibration references. No attempt has been made here to remove biases, only calibration coefficients available from the literature have been used. This encouraging results should trigger further quantitative use of these data for the generation of global products.

The analysis of the surface albedo consistency has revealed a good agreement between the products derived from the various satellites, despite the difference between their radiometers. Broadband surface albedos derived from identical radiometers like the GOES Imager or Meteosat/MVIRI are particularly consistent, with a mean bias not exceeding 2%. Largest biases are observed between Met-5 and GMS-5 due to residual cloud contamination during the processing of data from this former satellite. Comparison of this global product with other data sets such as those routinely derived from the Moderate-Resolution Imaging Spectroradiometer (MODIS) or the Multiangle Imaging SpectroRadiometer (MISR) onboard the Terra platform still needs to be performed.

These first results open therefore new avenue for the exploitation of the archived data for the generation of long time series of global surface albedo. In particular, it will be possible to derive at EUMETSAT with the GSA algorithm time series of surface albedos from Meteosat satellites at the  $0^{\circ}$  position from 1983 up to now, *i.e.*, more than two decades.

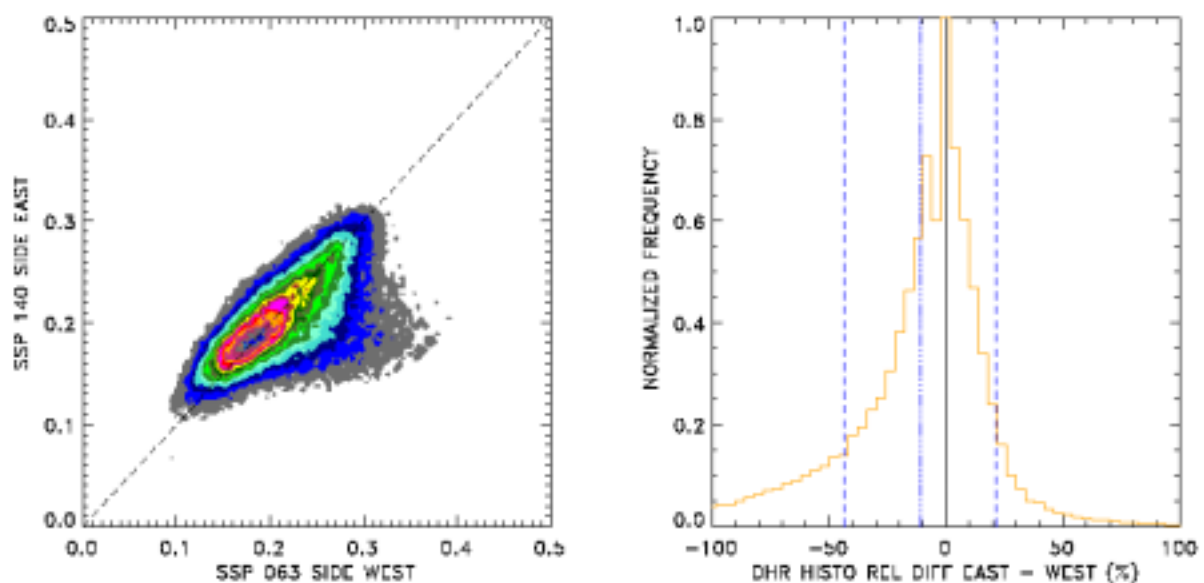


Figure 9: As Figure (6) but for Meteosat-5 (labelled SSP 063 SIDE WEST) and GMS-5 (labelled SSP 140 SIDE EAST).

The GSA algorithm could be made available to the CGMS members upon request for the processing of their own archive. The generation of the GSA product provides a quantitative mechanism to assess the quality of the archives, contributing thereby to the GCOS recommendations. The GSA algorithm could actually be applied to any geostationary satellites with a VIS band provided the following information is available:

- Hourly scan as a minimum temporal sampling;
- calibration information;
- the actual sub-satellite point at the time of acquisition;
- the acquisition time of each pixel;

- the radiometric noise (*e.g.*, standard deviation of the space count);
- the geographical coordinates of each pixel;
- the rectification accuracy estimation (*e.g.*, with respect to landmarks);
- the sensor spectral response and its uncertainty.

### **ACKNOWLEDGEMENTS**

The authors are grateful to the Japan Meteorological Agency (JMA) and the Satellite Services Group of the National Oceanic and Atmospheric Administration (NOAA) for providing the GMS-5 and GOES-8/-10 images and support their processing.

## References

- Ba, M. B., R. Frouin, S. E. Nicholson, and G. Dedieu (2001). Satellite-derived surface radiation budget over the African continent. Part I: estimation of downward solar irradiance and albedo. *Journal of Climate* 14, 45-58.
- Charney, J. G. (1975). Dynamics of deserts and droughts in the Sahel. *Quarterly Journal of the Royal Meteorological Society* 101, 193-202.
- Christy, J. R., R. W. Spencer, and W. D. Braswell (2000). MSU Tropospheric temperatures: Data set construction and radiosonde comparisons. *Journal of Atmospheric and Oceanic Technology* 17, 1153-1170.
- Dickinson, R. E. (1983). Land surface processes and climate-surface albedos, *Adv. Geophys.*, 25, 305-353, 1983. *Adv. Geophys.* 25, 305-353.
- GCOS (2003). Second report on the adequacy of the global observing systems for climate. Technical Report GCOS-82 (WMO/TD No 1143), World Meteorological Organization.
- Govaerts, Y., A. Lattanzio, B. Pinty, and J. Schmetz (2004). Consistent surface albedo retrieval from two adjacent geostationary satellites. *Geophysical Research Letters* 31, doi:10.1029/2004GL020418.
- Govaerts, Y., B. Pinty, M. Taberner, and A. Lattanzio (2005). Spectral conversion of surface albedo derived from Meteosat observations. *Geosciences and Remote Sensing Letters*, In Print.
- Govaerts, Y. M. and M. Clerici (2004). Evaluation of radiative transfer simulations over bright desert calibration sites. *IEEE Transactions on Geoscience and Remote Sensing* 42, 176-187.
- Govaerts, Y. M., M. Clerici, and N. Clerbaux (2004). Operational Calibration of the Meteosat Radiometer VIS Band. *IEEE Transactions on Geoscience and Remote Sensing* 42, 1900-1914.
- Jin, Y., C. B. Schaaf, F. Gao, X. Li, A. H. Strahler, W. Lucht, and S. Liang (2003). Consistency of MODIS surface bidirectional reflectance distribution function and albedo retrievals: 1. Algorithm performance. *Journal of Geophysical Research* 108, 4158, doi:10.1029/2002JD002803.
- Lattanzio, A., Y. Govaerts, and B. Pinty (2005). Consistency of surface anisotropy characterization with Meteosat observations. *Advanced Space Research*, In press.
- Le Borgne, P., G. Legendre, and A. Marsouin (2004). Meteosat and GOES-East Imager Visible Channel Calibration. *Journal of Atmospheric and Oceanic Technology* 21, 1701-1709.
- Martonchik, J. V., D. J. Diner, B. Pinty, M. M. Verstraete, R. B. Myneni, Y. Knyazikhin, and H. R. Gordon (1998). Determination of land and ocean re\_ective, radiative, and biophysical properties using multiangle imaging. *IEEE Transaction on Geosciences and Remote Sensing* 36, 1266-1281.
- Minnis, P., L. Nguyen, D. R. Doelling, D. F. Young, W. F. Miller, and D. P. Kratz (2002). Rapid calibration of operational and research meteorological satellite imagers. part I: evaluation of research satellite visible channels as references. *J. Atmos. Ocean. Technology* 19, 1233-1249.
- Nguyen, L., D. R. Doelling, P. J. Minnis, and J. K. Ayers (2004). Rapid technique to cross-calibrate satellite imager visible channels. In W. L. Barnes and J. J. Butler (Eds.), *Proceedings of 49th SPIE, Earth Observing Systems IX*, Denver, CO, pp. 227-235.
- Ohring, G. and A. Gruber (2001). Climate monitoring from operational satellites: accomplishments, problems, and prospects. *Advance in Space Research* 28, 207-219.
- Pinty, B., F. Roveda, M. M. Verstraete, N. Gobron, Y. Govaerts, J. V. Martonchik, D. J. Diner, and R. A. Kahn (2000a). Surface albedo retrieval from Meteosat: Part 1: Theory. *Journal of Geophysical Research* 105, 18099-18112.
- Pinty, B., F. Roveda, M. M. Verstraete, N. Gobron, Y. Govaerts, J. V. Martonchik, D. J. Diner, and R. A. Kahn (2000b). Surface albedo retrieval from Meteosat: Part 2: Applications. *Journal of Geophysical Research* 105, 18113-18134.
- Rahman, H., B. Pinty, and M. M. Verstraete (1993). Coupled surface-atmosphere re\_ectance (CSAR) model. 2. Semiempirical surface model usable with NOAA Advanced Very High Resolution Radiometer Data. *Journal of Geophysical Research* 98, 20,791-20,801.

- Robinson, D. A. (2000). Weekly Northern Hemisphere Snow Maps: 1966-1999. In AMS (Ed.), *12<sup>th</sup> Conference on Applied Climatology*, Asheville, NC, pp. 12-15.
- Rossow, W. B., F. Moshier, E. Kinsella, A. Arking, M. Desbois, E. Harrison, P. Minnis, E. Ruprecht, G. Seze, C. Simmer, and E. Smith (1985). ISCCP cloud algorithm intercomparison. *Journal of Climate and Applied Meteorology* 24, 877-903.
- Strong, A. E., E. J. Kearns, and K. K. Gjovig (2000). Sea surface temperature signals from satellites – an update. *Geophysical Research Letters* 27, 1667-1670.